Metabolomics Analysis of the Effects of Chelerythrine on Ustilaginoidea virens

Qinghui Wei (weiqinghuizi@126.com)
Institute of Plant Protection, Heilongjiang Academy of Agricultural Sciences
Weifeng Song
Institute of Plant Protection, Heilongjiang Academy of Agricultural Sciences
Zhiyong Li
Institute of Plant Protection, Heilongjiang Academy of Agricultural Sciences
Yaqing Pan
Institute of Plant Protection, Heilongjiang Academy of Agricultural Sciences
Xihai Zhai
Institute of Plant Protection, Heilongjiang Academy of Agricultural Sciences
Baoying Li
Institute of Plant Protection, Heilongjiang Academy of Agricultural Sciences
Zhanli Jiao
Institute of Plant Protection, Heilongjiang Academy of Agricultural Sciences

Research Article

Keywords: Rice false smut, Chelerythrine, Ustilaginoidea virens, Metabolomics, Metabolites, Metabolic pathways, UPLC-MS/MS, Random Forest analysis

Posted Date: March 1st, 2022

DOI: https://doi.org/10.21203/rs.3.rs-1207185/v1

Abstract

Background: Rice false smut (RFS), caused by *Ustilaginoidea virens*, is widely distributed in major rice-producing regions. Previous studies showed that treating RFS with chelerythrine can decrease fungus spore germination by 86.7% and induce fungal cell apoptosis.

Result: In the present study, the effects of chelerythrine on the metabolism of *U. virens* were explored using metabolomics, and analysing differentially expressed genes and altered metabolic pathways. A total of 1153 features (740 in positive ion mode, 401 upregulated, 339 downregulated; 413 in negative ionisation mode, 190 upregulated, 223 downregulated). The top 15 metabolites in Random Forest analysis were significantly different between groups. In positive ion mode, purine metabolism (map00230), phenylalanine metabolism (map00360), phenylalanine, tyrosine and tryptophan biosynthesis (map00400), pyrimidine metabolism (map00240) and nitrogen metabolism (map00910) were dominant. Alanine, aspartate and glutamate metabolism (map00250) and phenylalanine metabolism (map00360) were enriched in negative ion mode.

Conclusion: Differentially expressed genes and altered metabolic pathways of *U. virens* were effected by chelerythrine. The findings support future research on the prevention and treatment of RFS by chelerythrine, and provide a theoretical basis for targeted drug delivery.

1. Introduction

Rice false smut (RFS) is a fungal disease of rice affecting booting to heading stages. It is caused by infection of the flower organ by the pathogen *Ustilaginoidea virens.* The formation of dark green lumps on rice panicles is a typical symptom of this disease. RFS is widely distributed in major rice-producing countries in Asia, Africa, South America and Europe, especially in Asian countries (Brooks et al., 2009) RFS is now the main fungal disease in rice-producing areas in China (Fu et al., 2016). This disease not only affects the yield and quality of rice; it also produces toxins that are harmful to humans and livestock (Tanaka et al., 2008).

Chelerythrine is one of the most abundant alkaloids in the traditional herbal medicine Chelidonium majus L. It is an effective inflammatory inhibitor, and it is lethal to cancer cells without affecting normal cells, hence it can improve patient survival. Fan et al. (2009) found that chelerythrine has a strong inhibition effect on mycelial growth of crop pathogens such as *Fusarium oxysporum*, Anthrax and grey mold. Its pharmacological effects are well documented, including selective protein kinase C inhibition, and anti-inflammatory and anti-tumour activities (Hu et al., 2017; Saavedra et al., 2017; Zhu et al., 2018).

Among these, its anti-tumour activity has attracted the most attention, but the mechanism of inhibition is poorly understood, and this is a prerequisite for developing pesticide preparations. Our previous studies showed that chelerythrine inhibits fungus spore germination by up to 86.7%, and it induces apoptosis of *U. virens* cells (Wei et al., 2020). Developing chelerythrine as a green biological pesticide would be of great significance for agricultural production and environmental enhancement.

In the present study, the effects of chelerythrine on the metabolism of *U. virens* were investigated by metabolomics based on ultra-pressure liquid chromatography coupled to tandem mass spectrometry (UPLC-MS/MS) and analysing differentially expressed genes and altered metabolic pathways. Further studies on the mechanism of action could facilitate chelerythrine pesticide-based control of RFS.

2. Materials And Methods

2.1. Reagents, media and strains

We extracted chelerythrine as previously described (Wei et al., 2020). Methyl alcohol, methanoic acid and ammonium acetate were purchased from Thermo Fisher (Shanghai, China), and water was from Merck (Beijing, China).

U. virens strains were kindly provided by the Northeast Forestry University (Harbin, China) and cultured in potato sucrose (PS) medium (Guo et al., 2019) at 28°C.

2.2 Effects of chelerythrine on the metabolism of *U. virens*

U. virens was cultured in PS medium at 28°C for 10 days followed by incubation with 0.0075 mg/mL of chelerythrine for 24 h. Negative controls without chelerythrine were included in parallel. Samples were centrifuged, supernatants were discarded, and pellets were placed in EP tubes and resuspended in prechilled 80% methanol by vortexing on ice for 30 s. After sonication for 6 min, lysates were centrifuged at 5,000 rpm for 1 min at 4°C. The supernatant was freeze-dried and dissolved in 10% methanol, and an aliquot was injected into the LC-MS/MS system (Sellick et al., 2011; Yuan et al., 2012).

UPLC-MS/MS analyses were performed using a Vanquish UHPLC system (Thermo Fisher, Shanghai, China) coupled to an Orbitrap Q Exactive HF mass spectrometer (Thermo Fisher, Shanghai, China). Samples were injected onto a Hypesil Gold column (100 × 2.1 mm, 1.9 μm) over a 17 min linear gradient at a flow rate of 0.2 mL/min. Eluents for positive ion mode were buffer A (0.1% formic acid in water) and buffer B (methanol). Eluents for negative ion mode were buffer A (5 mM ammonium acetate, pH 9.0) and buffer B (methanol). The solvent gradient was 2% B for 1.5 min, 2–100% B over 12.0 min, 100% B for 14.0 min, 100–2% B over 14.1 min, 2% B for 17 min. The MS instrument was operated in positive and negative ion modes with a spray voltage of 3.2 kV, a capillary temperature of 320°C, a sheath gas flow rate of 40 arb and an aux gas flow rate of 10 arb. The method was carried out as previously described (Sellick et al., 2011; Yuan et al., 2012).

2.3 Data processing and metabolite identification

Raw data files generated by UPLC-MS/MS were processed using Compound Discoverer 3.1 (CD3.1, Thermo Fisher) to perform peak alignment, peak picking, and quantitation for each metabolite. The main parameters were retention time tolerance 0.2 min, actual mass tolerance 5 ppm, signal intensity tolerance 30%, signal/noise ratio 3, minimum intensity. Peak intensities were normalised to the total spectral intensity, and normalised data were used to predict the molecular formula based on additive ions,

molecular ion peaks and fragment ions. Peaks were matched using mzCloud (https://www.mzcloud.org/), mzVault and MassList databases to obtain accurate qualitative and relative quantitative results. The method was carried out as previously described (Sellick et al., 2011; Yuan et al., 2012).

2.4 Data analysis

Metabolites were annotated using the Kyoto Encyclopedia of Genes and Genomes (KEGG) database (https://www.genome.jp/kegg/pathway.html), the the human metabolome database (HMDB) (https://hmdb.ca/metabolites) and the lipid maps database (http://www.lipidmaps.org/). Data normalisation, principal component analysis (PCA), partial least squares discriminant analysis (PLS-DA), orthogonal partial least squares discriminant analysis (OPLS-DA), random forest (RF) and support vector machine (SVM) were performed with the R package MetaboAnalystR (Jasmine et al., 2018). To acquire normal distributions, the normalisation function in MetaboAnalystR was employed with MedianNorm, LogNorm and AutoNorm selected. We applied a univariate analysis (t-test) to calculate statistical significance (p-value). Metabolites with VIP (value importance in projection) > 1, $p < 0.05$ and log2 (Fold Change) > 1 were considered differential metabolites.

For clustering heatmaps, data were normalised as z-scores and plotted by Pheatmap package in R language. A volcano plots was used to filter metabolites of interest based on log2 (Fold Change) and -log10 (p-value), conducted by the R package ggplot2. Metabolites with $p < 0.05$ (t-test) were used to conduct an overrepresentation enrichment analysis (ORA), and the resulting KEGG pathways with $p < 0.05$ (ORA) were considered statistically significant.

3 Results

3.1 Metabolite content

We detected 1153 features (740 in positive and 413 in negative ionisation mode, respectively). The abundance of each metabolite in each sample was calculated, and an accumulation column chart was used for visualisation so that compositional and structural differences between metabolites in different groups could be intuitively compared. Figure 1 shows the top 20 most abundant metabolites.

Some of the identified metabolites play specific roles in organisms, such as hormones and vitamins. We annotated all metabolites using KEGG database BR08001 to infer the biological roles played by the metabolites. The number of terms related to biological roles was then counted and a column chart was drawn (Fig. 2).

Metabolites detected by positive ion mode were divided into nine categories; control vs. treatment peptides were 46.27% vs. 58.55%, nucleic acids were 43.39% vs. 27.62%, vitamins and cofactors were 4.56% vs. 4.23%, and carbohydrates were 3.89% vs. 7.85%. Metabolites detected by negative ion mode were divided into eight categories; control vs. treatment organic acids were 50.45% vs. 49.76%,

carbohydrates were 21.51% vs. 34.13%, nucleic acids were 9.14% vs. 5.40%, lipids were 8.14% vs. 6.32%, and peptides were 6.85% vs. 3.69%.

3.2 Principal component analysis

PCA was performed on the identified metabolites, a scatter diagram was drawn from the results, and structural differences between metabolites in different samples were inferred. Where the distributions of groups are clearly in different areas, this indicates that metabolite structures are quite different. In the PCA diagram (Fig. 3), each point corresponds to a sample, and the distance between two points is proportional to the differences of in metabolite structures between two groups (Euclidean distance). Different groups are marked in different colours, and the area marked by the ellipse is the 95% confidence region. In positive ion mode, the first principal component accounts for 67.30% of the variation, and the second principal component accounts for 8.10%. In negative ion mode, the first principal component accounts for 67.80%, and the second principal component accounts for 10.40%.

3.3 Screening and analysis of differential metabolites

In order to accurately identify differential metabolites, an OPLS-DA model was used to analyse the metabolomic data. The R^2Y and Q^2 values were close to 1 (in positive ion mode, $R^2X = 0.744$, $R^2Y = 1$, $Q^2 = 0.995$; in negative ion mode, $R^2X = 0.776$, $R^2Y = 0.999$, $Q^2 = 0.994$). This indicates that the OPLS-DA model was stable and highly reliable for this dataset, and could be confidently used to explore differences between treatment and control groups (Fig. 4).

In positive ion mode, 740 differentially abundant metabolites were identified, of which 401 were upregulated and 339 were downregulated; in negative ion mode, 413 differentially abundant metabolites were identified, of which 190 were upregulated and 223 were downregulated (Fig. 5).

3.4 Random forest analysis

In random forest analysis, mean decrease in accuracy and mean decrease in gini are used to measure the importance of discriminant groupings of metabolites. The value of a metabolite is changed to a random number, and the reduction in prediction accuracy of the random forest is the mean decrease accuracy; The mean decrease in gini is the effect of a metabolite on the heterogeneity of observed values at all nodes of the classification tree; the larger these two values are, the greater the importance of metabolites in the random forest. Figure 6 shows the 15 most important metabolites in the random forest, and these metabolites should be significantly different between groups.

In positive ion mode, pc (18:3e /22:6) is the most important metabolite. Compared with control groups, pc (18:3e /22:6), n-tetradecanamide, 9-oxo-ode, n1-(2-amino-2-oxoethyl)-2-phenoxyacetamide, 2-phenylglycine, pc (18:0/19:2) and isoproterenol were upregulated in treatment groups. Meanwhile, pantothenic acid, feruloyl putrescine, pc(16:2e/2:0), TNK, ILK, 3-(3,4-dihydroxyphenyl) propanoic acid, 1-[5-(2-phenyleth-1-ynyl)-2-thienyl]ethan-1-one oxime, and geranyl pp were less abundant. In negative ion

mode, 5-(tert-butyl)-2-methyl-n-(5-methyl-3-isoxazolyl)-3-furamide was the most important metabolite. Compared with control groups, melatonin, 2-(formylamino)benzoic acid, undecanedioic acid, palmitic acid, n-acetyl-l-ornithine, d-glucuronic acid, sucrose, and 15(R), 19(R)-hydroxy prostaglandin F1α were upregulated in treatment groups. Meanwhile, 5-(tert-butyl)-2-methyl-n-(5-methyl-3-isoxazolyl)-3-furamide, mag (18:4), 12-hydroxydodecanoic acid, phloretin, sorbitan monostearate, 5'-deoxy-5'-(methylthio) adenosine and 5-s-cysteinyldopaquinone were downregulated.

3.5 Pathway enrichment analysis

The purpose of enrichment analysis is to search for biological pathways that play key roles in a biological process, and thereby reveal the basic molecular mechanisms of the biological processes. Prior to enrichment analysis, we selected certain metabolites, mainly those that differed significantly between groups (t-test, P&LT 0.05), and explored which metabolic pathways (KEGG species-specific metabolic pathways, slightly different metabolic pathways in different species) these metabolites are related to by calculating the ORA and *p*-values of the metabolic pathways, In this way, we determined whether the metabolites of concern (significantly differential metabolites) were significantly enriched in these metabolic pathways. Figure 7 shows the metabolic pathways with significant enrichment of differential metabolites. These metabolic pathways may be important in the biological processes studied.

According to the fold enrichment value ordered from higher to lower, in positive ion mode, differential metabolites were significantly enriched in 33 metabolic pathways, the top six of which were phenylalanine, tyrosine and tryptophan biosynthesis, biotin metabolism, phenylalanine metabolism, nitrogen metabolism, pyrimidine metabolism, and pantothenate and CoA biosynthesis. In negative ion mode, differential metabolites were significantly enriched in 52 metabolic pathways, the top six of which were alanine, aspartate and glutamate metabolism, lipoic acid metabolism, phenylalanine metabolism, cyanoamino acid metabolism cyanoamino, D-Arginine and D-ornithine metabolism, and pantothenate and CoA biosynthesis.

3.6 Topology analysis

The effects of metabolites on metabolic pathways can be estimated by topology analysis, and the effects can be measured by impact. For example, if there are no other metabolites or genes downstream of a metabolite in a metabolic pathway, then we can deduce that the effect of this metabolite on the metabolic pathway is negligable. Conversely, if a metabolite is very close upstream and there are many other metabolites and genes downstream, then the metabolite can be considered to have a large effect on the metabolic pathway.

Topological analysis is often combined with enrichment analysis to determine whether a metabolic pathway plays a key role in the biological process under study. The metabolic pathways in blue in Fig. 8 are prominent in the ORA results, and the vertical axis shows the impact of these metabolic pathways in the topological analysis. In positive ion mode, purine metabolism (map00230), phenylalanine metabolism (map00360), phenylalanine, tyrosine and tryptophan biosynthesis (map00400), pyrimidine metabolism (map00240) and nitrogen metabolism (map00910) play key roles. Alanine, aspartate and

glutamate metabolism (map00250) and phenylalanine metabolism (map00360) play key roles in negative ion mode.

3.7 Metabolic pathway mapping

Metabolic pathway mapping can intuitively reflect upstream and downstream relationships, modes of action, and the metabolic pathway topological structure of metabolites, as well as identify genes associated with metabolites. Figure 9 shows metabolic pathways containing only metabolites, and red metabolites are the metabolites of concern (i.e. metabolites with significant differences between groups).

4. Discussion

In this study, UPLC-MS/MS was employed to investigate changes in metabolism in *U. virens* following treatment with chelerythrine. PCA and OPLS-DA results showed revealed obvious differences between treatment and control groups, and combining differential metabolites and enriched pathways showed that treatment with chelerythrine reduced stress resistance of the pathogen, and eventually led to cell apoptosis, consistent with previous reports (Wei et al., 2020).

4.1 Chelerythrine treatment alters the abundance of key metabolites

We identified the 15 most important metabolites in the random forest analysis. Phosphatidylcholine (PC) is the most abundant phospholipid in the eukaryotic cell membrane. It plays an important role in cell proliferation and differentiation, and it is of great significance in controlling the cell cycle and apoptosis. Some diseases, such as cancer, Alzheimer's disease and stroke, are closely related to abnormal PC metabolism. A change in PC content indicates a change in the resistance of pathogens to external stimuli. Thus, PC can serve as a target for the prevention and treatment of RFS (Chang et al., 2006). The organic acid 2-phenylglycine and its derivatives can inhibit fungal mycelia growth and spore germination. The content of 2-phenylglycine was increased following chelerythrine treatment, indicating that the growth of *U. virens* was inhibited, consistent with laboratory results (Yoshida et al., 2021). Pantothenic acid is a disease resistance metabolite, and its downregulation weakens the ability of pathogens to resist external drug stress (Corinti et al., 2021). Feruloyl putrescine, a diamine that is toxic to the human body, is mainly synthesised by microorganisms through ornithine decarboxylase and arginine decarboxylase pathways, and its downregulation diminishes virulence (Marine et al., 2019).

Negative ion mode identified melatonin, an indole hormone. Melatonin protects cell structure, prevents DNA damage, and reduces peroxide levels by scavenging free radicals, resisting oxidation, and inhibiting lipid peroxidation. Melatonin has obvious antagonistic effects on tissue damage caused by peroxidation and free radicals produced by exogenous substances. Following chelerythrine treatment group, melatonin levels were increased, indicating that defences were triggered in pathogen cells (Tang et al., 2021).

Undecanedioic acid exerts important effects on key processes such as cell wall function, membrane assembly, lipid metabolism, pathogenesis, and even mRNA processing. Undecanedioic acid was more abundant in the chelerythrine treatment group, indicating that the drug affected cell membrane synthesis (Antonio et al., 2021). Conversely, chelidonine treatment lowered the abundance of 5-(tert-butyl)-2-methyl-N-(5-methyl-3-ISoxazolyl)-3-furamide, which regulates cell growth (BIAN et al., 2008). MAG, a lipid metabolite that participates in cell membrane synthesis and is linked to self-repair, was downregulated by chelerythrine treatment (Xu, 2019).

4.2 Chelerythrine treatment alters metabolic pathways

The key role of phenylalanine metabolism (map00360) was detected in both positive and negative ion modes. Specifically, 2-(formylamino)benzoic acid, which was upregulated by chelerythrine treatment, was one of the top 15 metabolites in random forest analysis, and this compound has antifungal activity. Adding uridine 5'-monophosphate can block conserved phosphorylation sites in the activation loop of BIK1 and RIPK, reducing their kinase activity, and consequently inhibiting downstream signalling (Feng et al., 2012). Deoxycytidine may restore MEG3 mRNA expression levels by reversing MEG3 promoter hypermethylation in bladder cancer cells, thereby inducing apoptosis (Jiang et al., 2021). 5-methylcytosine (m5C) is a common epigenetic modification with roles in eukaryotes, and m5C-related genes play a critical role in tumour progression in ovarian cancer (Wang and Gao et al., 2021). Further analysis of m5C methylation could provide a novel targeted therapy for treating ovarian cancer.

In this study, metabolomics was used to study differences in metabolites and metabolic pathways in *U. virens* following treatment with chelerythrine. The results could support the prevention and treatment of RFS, and provide a theoretical basis for targeted drug delivery.

Declarations

Ethics approval and consent to participate: All methods were performed in accordance with the relevant guidelines and regulations.

Consent for publication: Not applicable

Availability of data and materials: All of the material is owned by the authors and/or no permissions are required. Raw data was provided in this picture, it can be obtained by scanning with Baidu web disk.

Competing interests: The authors declare no competing financial interests.

Funding: This research was funded by subject of Institute of Plant Protection of Heilongjiang Academy of Agricultural Sciences (Harbin, China).

Author contributions: Qinghui Wei proposed the conceptualization, methodology, writing-review & editing, resources, writing-original draft preparation and gained acquisition of the financial support for the project leading to this publication. Investigation, formal analysis, data curation were performed by Qinghui Wei, Weifeng Song, Zhiyong Li, Yaqing Pan, Xihai Zhai, Baoying Li and Zhanli Jiao. All authors have read and agreed to the published version of the manuscript.

Acknowledgements: *U. virens* strains were kindly provided by Northeast Forestry University (Harbin, China)

References

1. Brooks, S.A.; Anders, M.M.; Yeater, K.M. Effect of cultural management practices on the severity of false smut and kernel smut of rice. Plant dis, 2009, 93: 1202–1208
2. Rong, T.; Wang, J.; Lu, D.H.; et al. Research progress of rice smut at home and abroad. Chinese Agricultural Science Bulletin, 2016, 32(12): 189–194.
3. Tanaka, E.; Ashizawa, T.; Sonoda R.; et al. Villosiclava virens gen. nov., comb. nov., teleomorph of *Ustilaginoidea virens*, the causal agent of rice false smut. Mycotaxon, 2008, 106(1): 491–501.
4. Fan, H.Y.; Xue, G.H.; Lu, C.; et al. Extraction and antibacterial activity of celandine from Celandine. Food Science, 2009, 30(24):126–129.
5. Hu, B.; Xu, G.; Zheng, Y.; et al. Chelerythrine Attenuates Renal Ischemia/Reperfusion-induced Myocardial Injury by Activating CSE/H2S via PKC/NF-κB Pathway in Diabetic Rats. Kidney & Blood Pressure Research. 2017, 42(2), 379–388.
6. Saavedra, A.; Fernández, G.; Sara; et al. Chelerythrine promotes Ca2 + dependent calpain activation in neuronal cells in a PKC-independent manner. BBA-General Subjects. 2017, 1861(4), 922–935.
7. Zhu, Y.; Pan, Y.; Zhang, G.; et al. Chelerythrine Inhibits Human Hepatocellular Carcinoma Metastasis in Vitro. Biol Pharm Bull. 2018, 41.
8. Wei, Q.H.; Cui, D.Z.; Liu, X.F. et al. In vitro antifungal activity and possible mechanisms of action of chelerythrine. Pesticide Biochemistry and Physiology, 2020, 164(2020):140–148.
9. Guo, W.W.; Gao, Y.X.; Yu, Z.M.; et al., 2019. The adenylate cyclase UvAc1 and phosphodiesterase UvPdeH control the intracellular cAMP level, development, and pathogenicity of the rice false smut fungus *Ustilaginoidea virens*. Fungal Genetics and Biology, 129:65–73.
10. Sellick, C. A.; Hansen, R.; Stephens, G.M.; et al. Metabolite extraction from suspension cultured mammalian cells for global metabolite profiling. Nature Protocol, 2011, 6(8):1241–9.

11. Yuan, M.; Breitkopf, S.B.; Yang, X.; et al. A positive/negative ion-switching, targeted mass spectrometry-based metabolomics platform for bodily fluids, cells, and fresh and fixed tissue. Nature Protocols, 2012, 7(5):872–81.
12. Jasmine, C.; Jianguo, X.; Oliver, S. MetaboAnalystR: an R package for flexible and reproducible analysis of metabolomics data. Bioinformatics, 2018.
13. Chang, P.A.; Qin, W.Z.; Wei, J.M. Lecithin and cell cycle. Chinese journal of biochemistry and molecular biology, 2006 (12): 947–952.
14. Yoshida, S.; Honjo, T.; Iino, K.; et al. Generation of human-induced pluripotent stem cell-derived functional enterocyte-like cells for pharmacokinetic studies. Stem Cell Reports, 2021, 16(2).
15. Corinti, D.; Chiavarino, B.; Scuderi, D.; et al. Molecular Properties of Bare and Microhydrated Vitamin B5–Calcium Complexes. International Journal of Molecular Sciences, 2021, 22(2):692.
16. Marine, V.; Marjolaine; et al. A common metabolomic signature is observed upon inoculation of rice roots with various rhizobacteria. Journal of integrative plant biology, 2019.
17. Tang, H.W.; Shi, X.Y; Zhu, P.F.; et al. Melatonin inhibits gallbladder cancer cell migration and invasion via ERK-mediated induction of epithelial-to-mesenchymal transition. Oncology letters, 2021, 22(2).
18. Antonio, R.; Maíra, P.M.; Tamires, A.; et al. Reassessing the Use of Undecanoic Acid as a Therapeutic Strategy for Treating Fungal Infections. Mycopathologia, 2021, 186(3).
19. Bian, W.D.; Chai, A.; Xu, S.R.; et al. Synthesis and herbicidal activity of 1,3, 4-thiadiazole derivatives of 5-fluorophenyl furfuramide. Organic Chemistry, 2008, 28(008):1475–1478.
20. Xu, M.M. Study on antibacterial mechanism of monoglycerol galactosyl laurate against Bacillus spp. Nanjing agricultural university, 2019.
21. Feng, F.; Yang, F.; Rong, W.; et al. A Xanthomonas uridine 5'-monophosphate transferase inhibits plant immune kinases. Nature, 2012, 485(7396), 114–8.
22. Jiang, Y.C.; Chen, B., Wu, J.B.; et al. Effects of 5-aza-2-deoxycytiside on MEG3 promoter hypermethylation reversal and apoptosis of bladder cancer cells. Journal of Zhejiangmed, 2021, 43(12):1284–1286 + 1294 + 1368.
23. Wang, L.; Gao, S. Identification of 5-methylcytosine-related signature for predicting prognosis in ovarian cancer. Biological research, 2021, 54(1): 18–18.

Figures

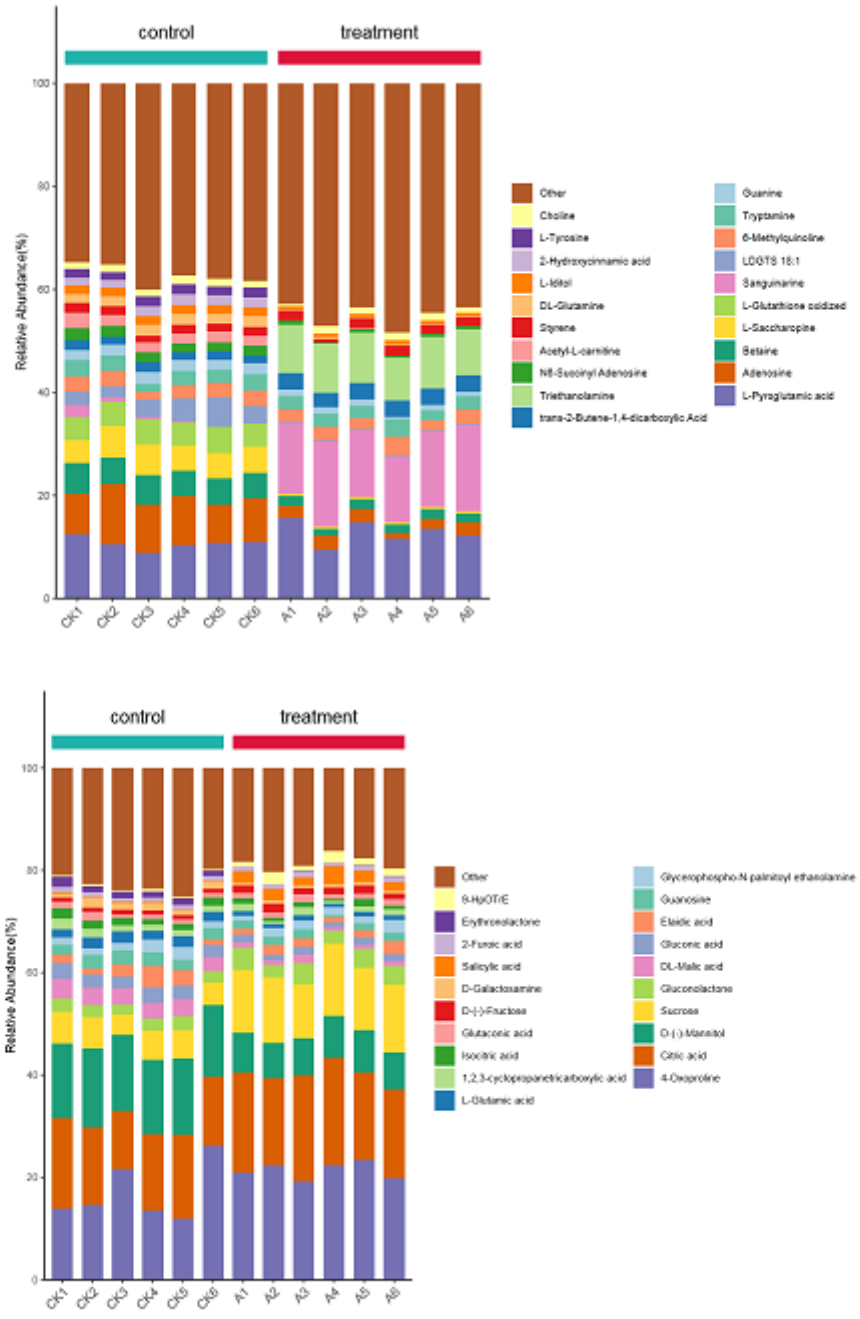

Figure 1

Column chart of metabolite abundance for the top 20 differential metabolites following chelerythrine treatment. The abscissa is the sample name, sorted according to the grouping order, and different samples groups are marked with different colours. The ordinate is the percentage content of each metabolite. The sequences of columns corresponding to metabolites from top to bottom is consistent with the legend. The box above is for positive ion mode and the box below is for negative ion mode.

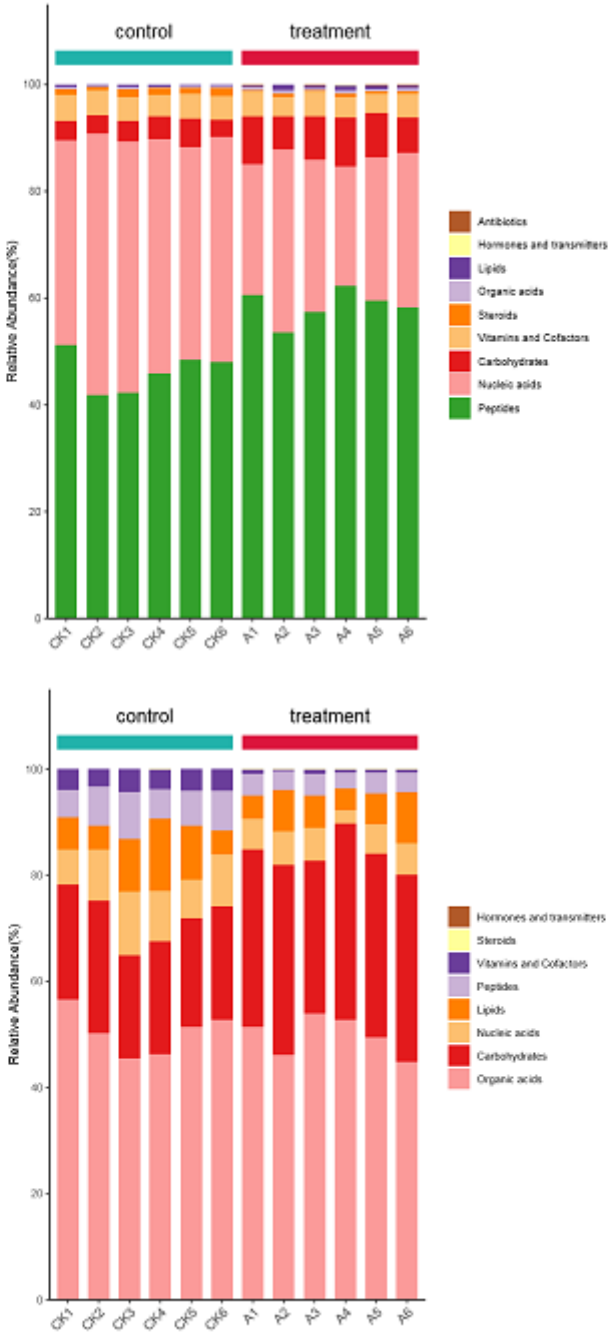

Figure 2

Histogram of differential metabolites playing key biological roles. The abscissa is the sample name, sorted according to the grouping order, and the different sample groups are marked with different colours. The ordinate is the percentage of each biological role. The box above is for positive ion mode and the box below is for negative ion mode.

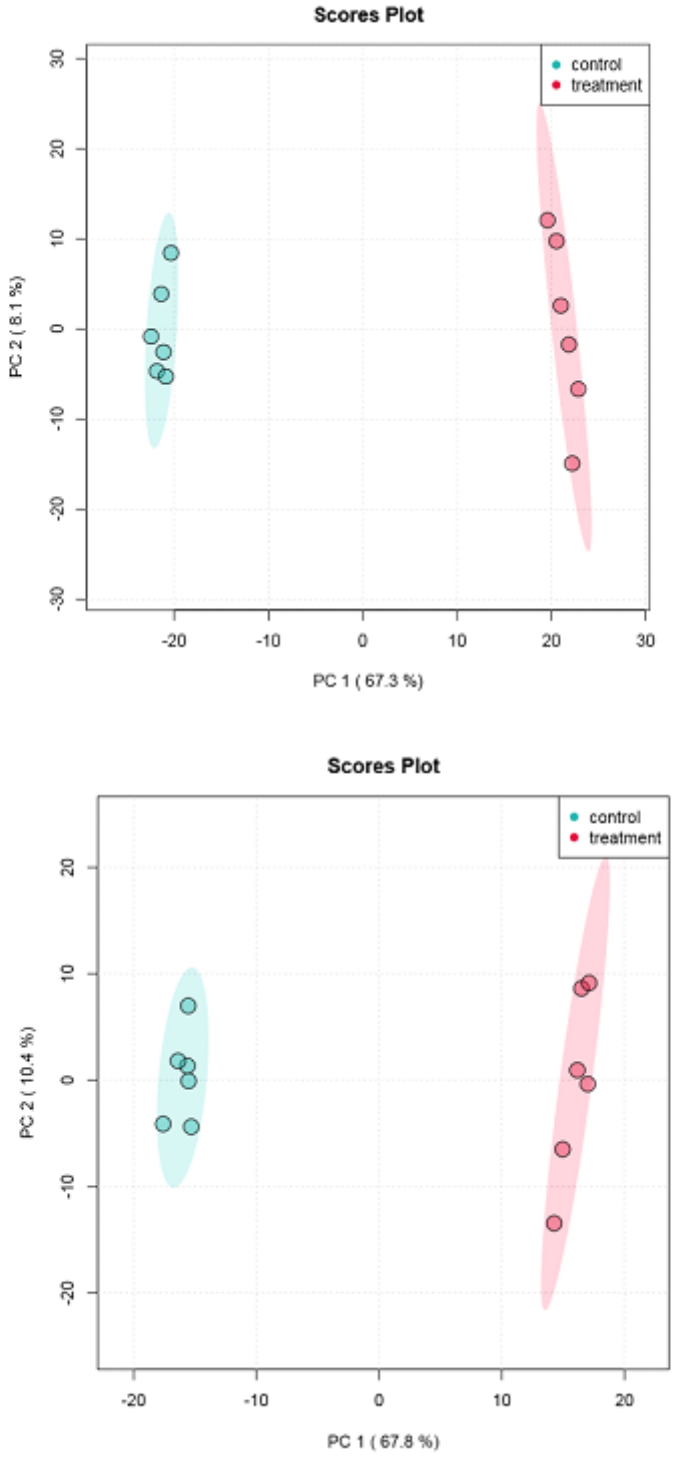

Figure 3

Principal component analysis. The box above is for positive ion mode and the box below is for negative ion mode.

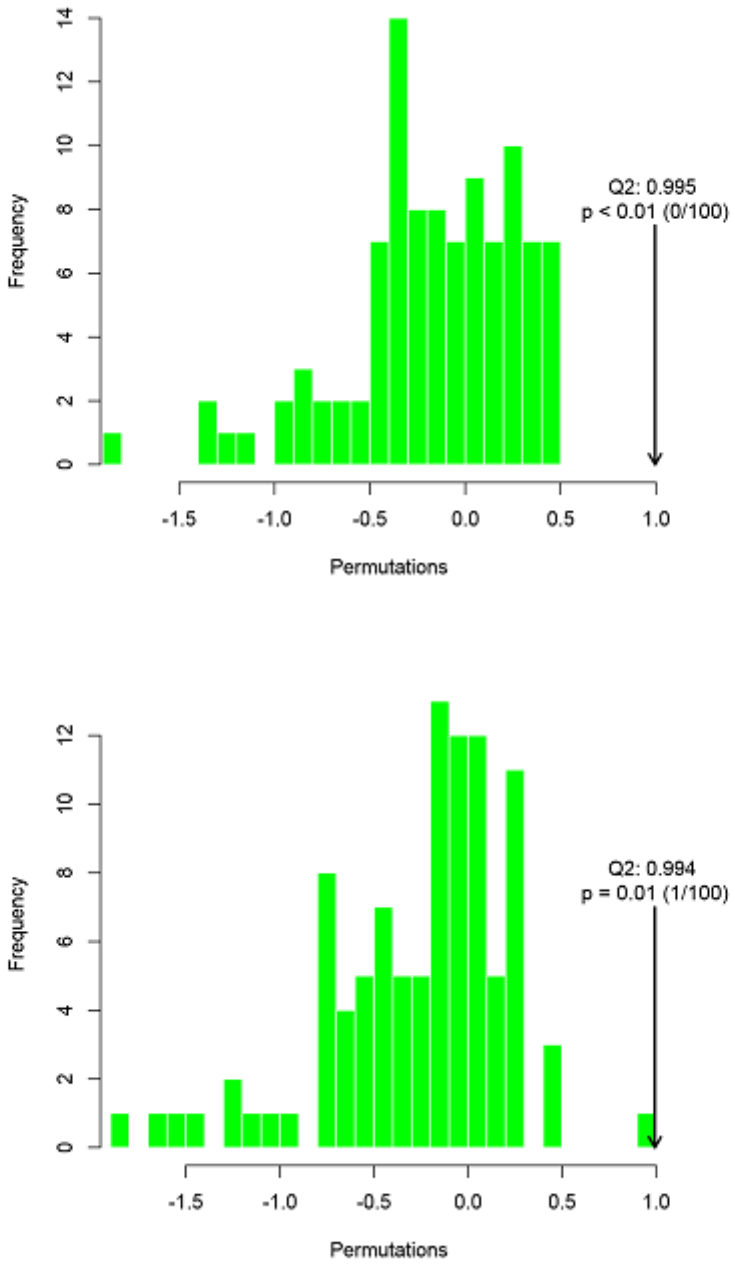

Figure 4

Permutation tests for the OPLS-DA model. Positive ion mode is shown above and negative ion mode is shown below.

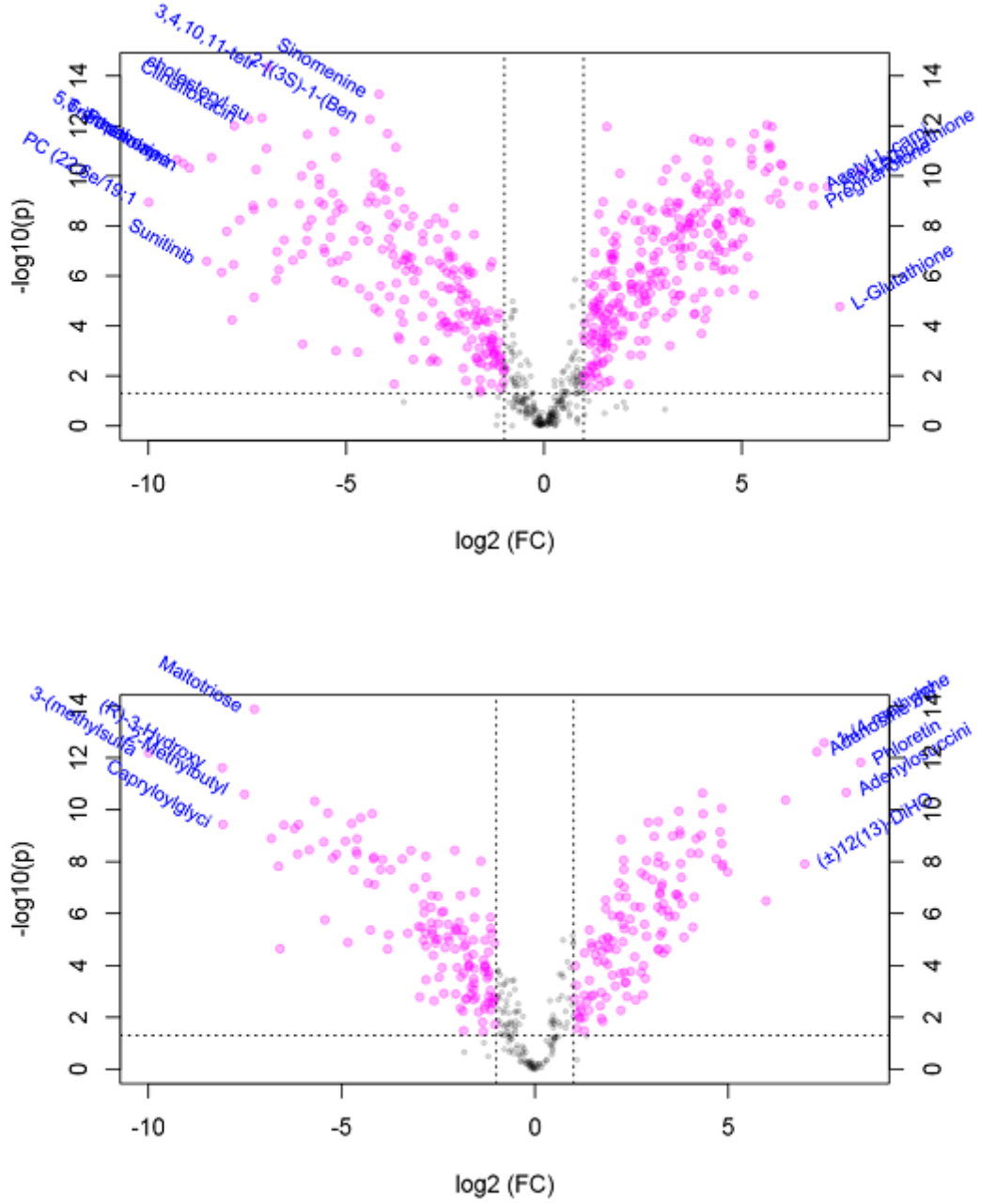

Figure 5

Volcano plot of differentially abundant metabolites (DAMs) for chelerythrine treatment vs. control groups. (a) Positive ion mode. (b) Negative ion. The y-axis is the *p*-value and the x-axis is the fold change (FC); *p* <0.05 and FC ³1 were used as thresholds to determine the significance of DAMs (dotted line).

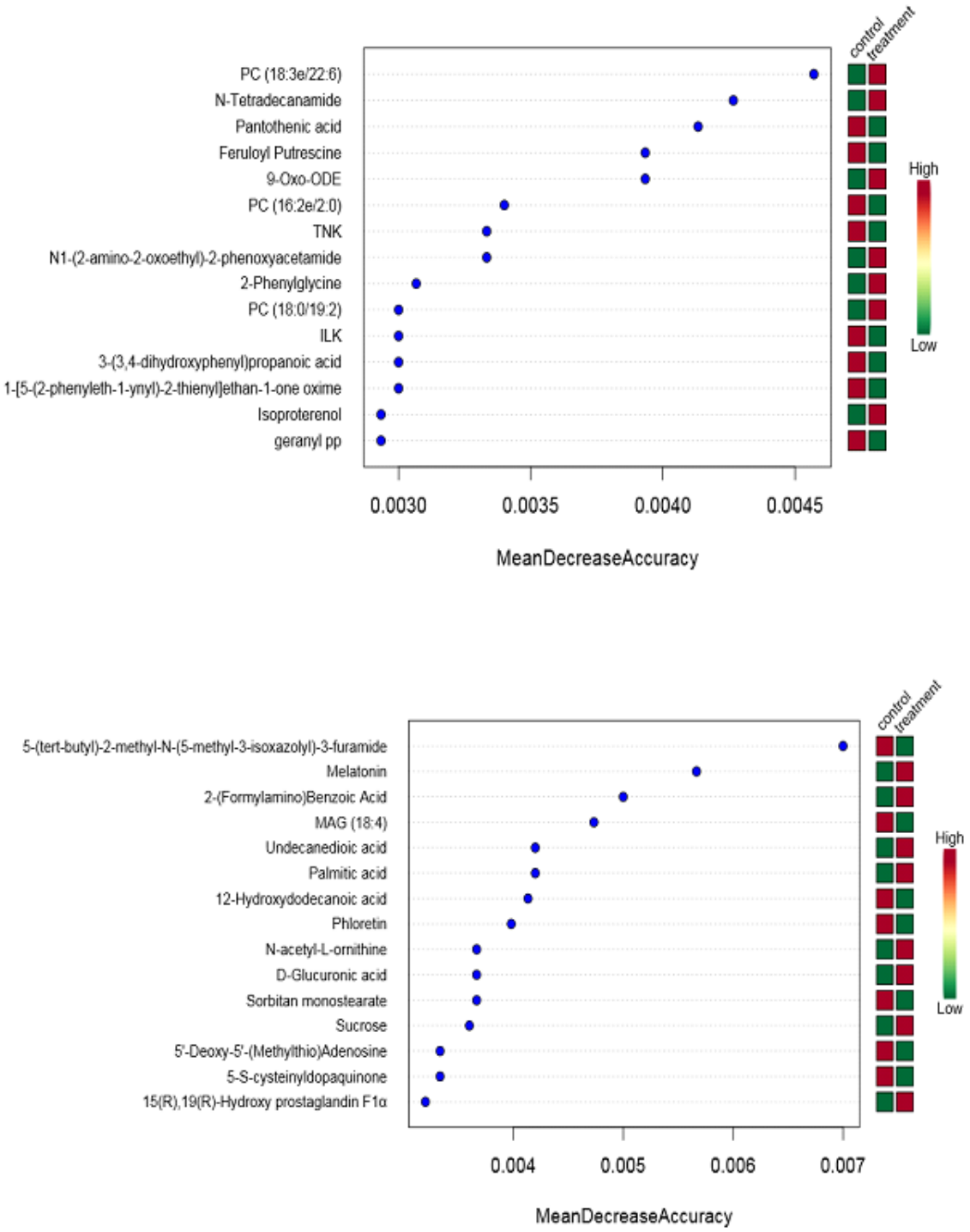

Figure 6

The top 15 differential metabolites according to random forest analysis. The x-axis on the left is the mean decrease in accuracy, which measures the importance of a metabolite in a random forest. The figure on the right is a heatmap of the top 15 metabolites in both groups. The box above is for positive ion mode and the box below is for negative ion mode.

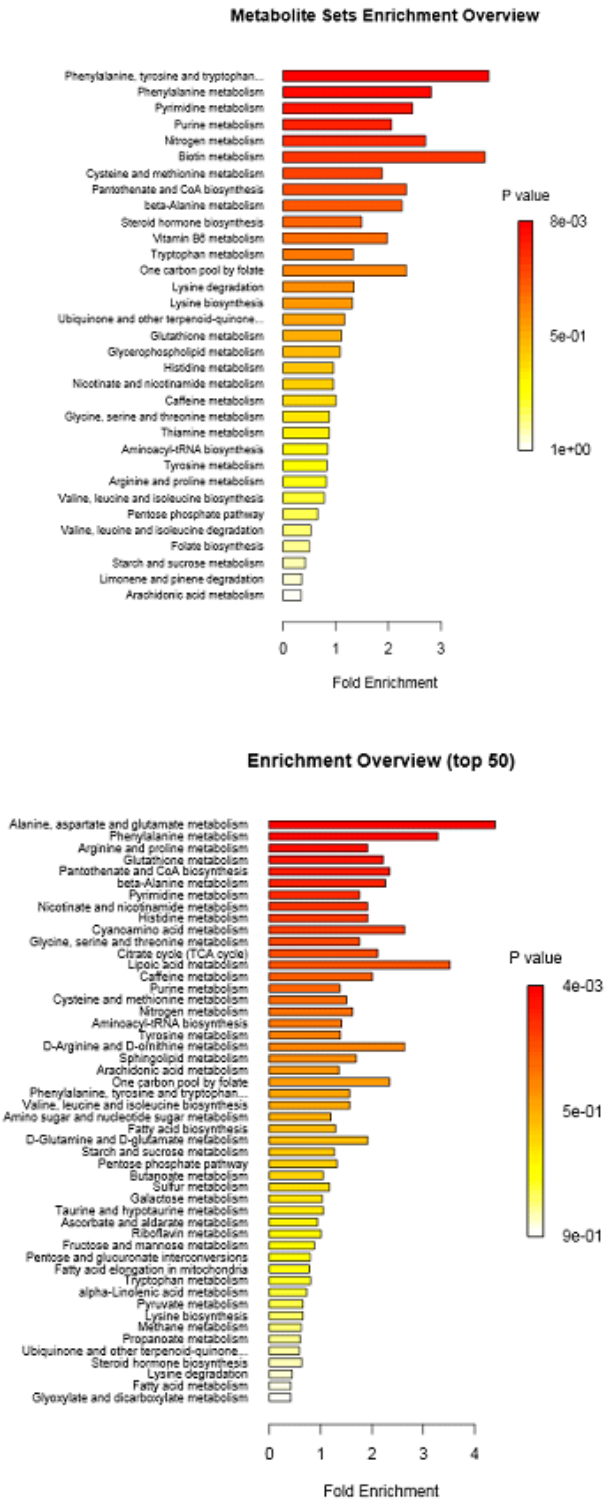

Figure 7

ORA enrichment analysis. The horizontal coordinate is the enrichment multiple, which represents the *p*-value of observed/theoretical metabolite number in the metabolic pathway; the darker the colour, the smaller the *p*-value. The box above is for positive ion mode and the box below is for negative ion mode.

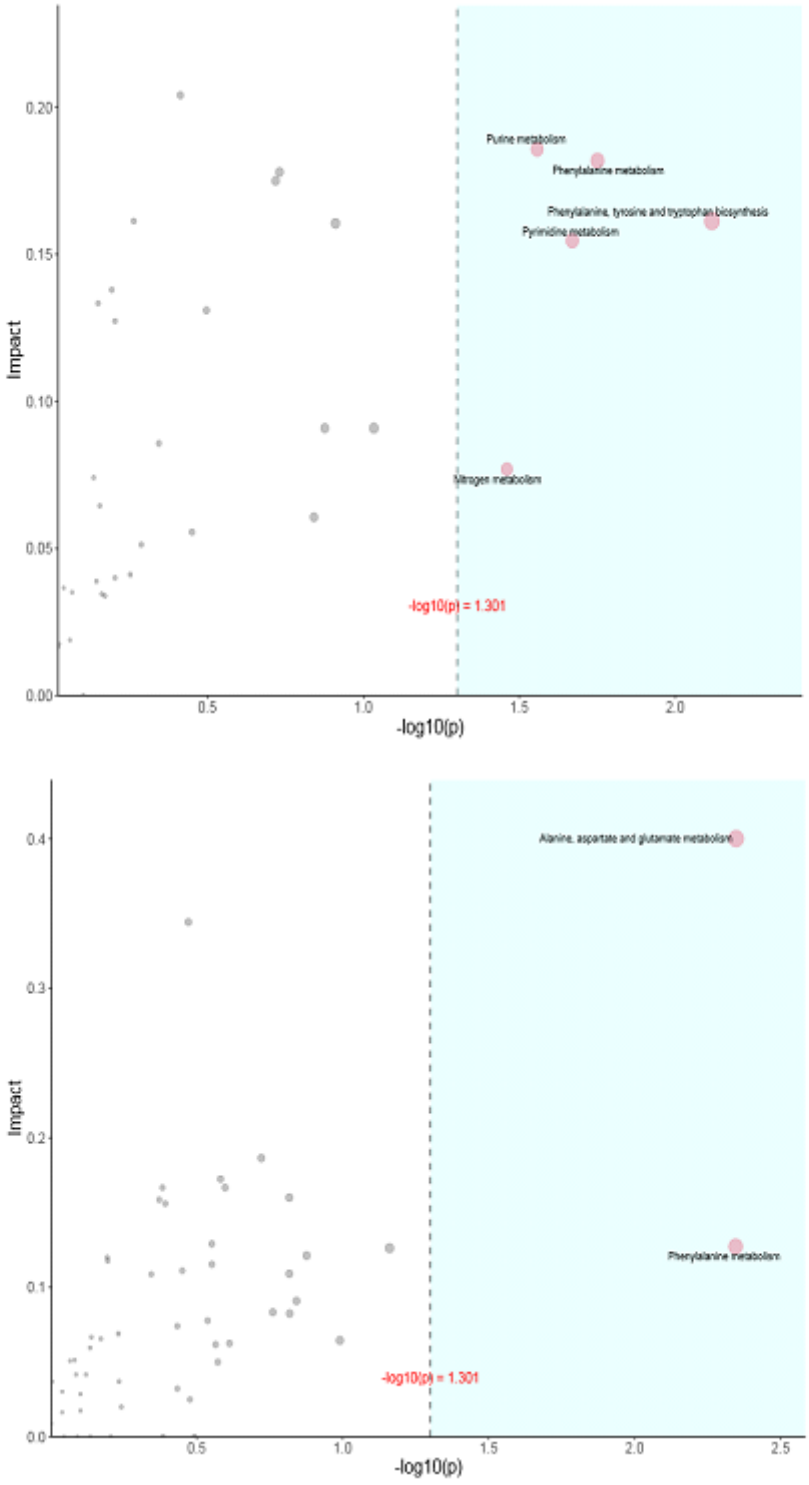

Figure 8

ORA enrichment and topological analyses. The horizontal coordinate shows the ORA analysis p-values, and the blue area is significant (P&LT 0.05). The vertical axis is the topology analysis impact. The box above is for positive ion mode and the box below is for negative ion mode.

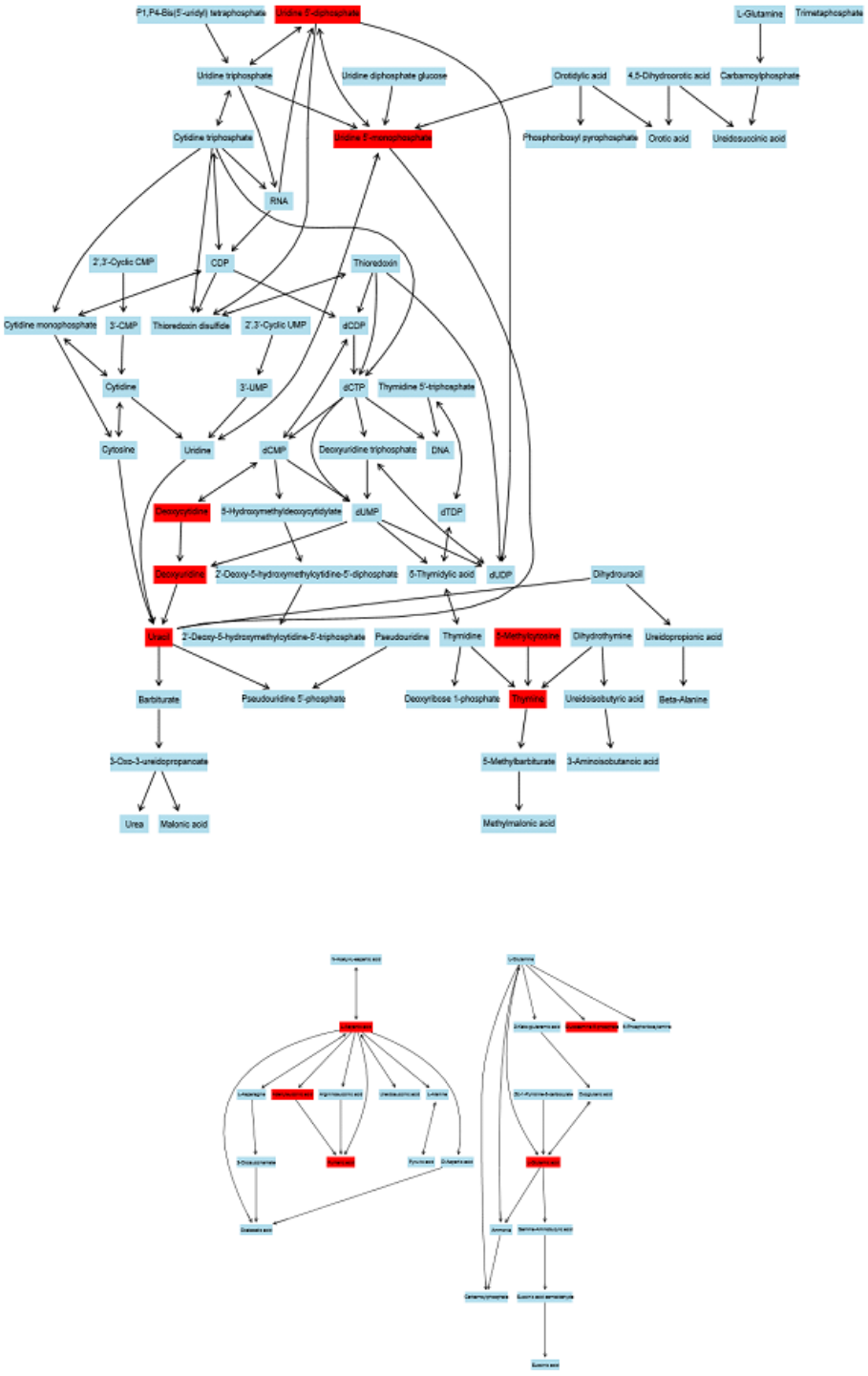

Figure 9

Pyrimidine metabolism pathways (containing only metabolites). The box above is for positive ion mode and the box below is for negative ion mode.